J. Fluid Mech. (1996), vol. 326, pp. 265–284

Nonlinear development of flow in channels with non-parallel walls

By O. R. TUTTY

Department of Aeronautics and Astronautics, University of Southampton, Southampton SO17 1BJ, UK

(Received 10 July 1995 and in revised form 18 April 1996)

In Jeffery–Hamel flow, the motion of a viscous incompressible fluid between rigid plane walls, unidirectional flow is impossible if the angle between the walls exceeds a critical value of $2\alpha_2$ which depends on the Reynolds number. In this paper the nonlinear development of the flow near this critical value is studied through numerical solutions of the two-dimensional Navier–Stokes equations for flow in divergent channels with piecewise straight walls. It is found that if the angle between the walls exceeds $2\alpha_2$ then Jeffery–Hamel flow does not occur, and the solution takes the form of a large-amplitude wave with eddies attached alternately to the upper and lower walls. When viewed in the appropriate coordinate system, far downstream the wave has constant wavelength and strength, although, physically, there is a linear increase in wavelength with distance downstream, i.e. the wavelength is proportional to the channel width. If the angle between the walls is less than $2\alpha_2$, then the existence (or otherwise) of the wave depends on the conditions near the inlet, in particular the local geometry of the channel. Jeffery–Hamel flow is obtained downstream of the inlet for angles well below $2\alpha_2$, but close to but below the critical value, solutions have been obtained with the wave extending (infinitely) far downstream. The wavelengths obtained numerically were compared with those from linear theory with spatially developing steady modes. No agreement was found: the wavelengths from the steady Navier–Stokes solutions are significantly larger than that predicted by the theory. However, in other important aspects the results of this study are consistent with those from previous studies of the development/existence of Jeffery–Hamel flow, in particular as regards the importance of the upstream conditions and the subcritical nature of the spatial development of the flow near the critical boundary in the Reynolds number–wall angle parameter space.

1. Introduction

Jeffery–Hamel flows, which are among the best known exact solutions of the Navier–Stokes equations, give the steady two-dimensional laminar flow of an incompressible viscous fluid between two rigid planes with a line source or sink at the intersection between the planes. They depend on two dimensionless parameters: α, the semi-angle between the planes (by convention the angle between the planes is taken as 2α), and the Reynolds number Re. For such an apparently simple problem, there is a rich structure of possible flow patterns, with many possible solutions for each pair of values of α and Re, involving pure inflow or outflow, or flows with a combination of inflow and outflow. Since they were discovered by Jeffery (1915) and Hamel (1916), there have many studies of Jeffery–Hamel (JH hereafter) flow. Of

particular interest to the present study are those by Fraenkel (1962, 1963), Sobey & Drazin (1986) and Banks, Drazin & Zaturska (1988).

In this paper we will consider the nonlinear development of the flow in non-uniform channels in which JH flow might be expected to occur, by generating detailed numerical solutions of the two-dimensional Navier–Stokes equations. The geometry used is not that of two inclined planes, but of a uniform channel at the inlet, followed by straight walls at a constant angle. Both symmetric and asymmetric channels are considered, as are those with and without a step at the point the channel changes shape. When necessary (on numerical grounds), there is a second change of shape downstream so that there is a uniform outlet. The geometry for a asymmetric channel is shown in figure 1 below. A symmetric channel is generated by reflection about the lower wall. This geometry is relatively simple, but has a number of useful features, both in terms of the definition of the problem and in the details of the numerical scheme. The flow can develop naturally from the incoming Poiseuille flow, and, when necessary, revert to Poiseuille flow far downstream, giving straightforward upstream and downstream boundary conditions which are physically sensible. However, by making the channel sufficiently long, it is possible for JH flow to develop naturally in the non-parallel section of the channel. With a symmetric channel, a symmetric solution can be generated by forcing symmetry, and a symmetry breaking process will be necessary to produce a non-JH flow far downstream of the initial change in shape, whereas for an asymmetric channel, the asymmetric disturbance to the flow generated by the shape in shape must decay for JH flow to occur. Finally, by increasing the size of the step, the effect of changing the size of the disturbance to the flow can be studied. As will be seen below, for certain regions in the (Re, α) parameter space, the details of the geometry will have a significant effect on the eventual flow pattern downstream of the change from parallel to non-parallel walls, i.e. far downstream of the change in shape near the inlet, more than one flow pattern can be generated for each set of (Re, α).

Although JH flows exist both for convergent and divergent channels, we will be concerned mainly with divergent channels, as these produce much more interesting results in the present context, and unless specifically mentioned, all remarks below will be assumed to refer to divergent channels.

Fraenkel (1962, 1963) classified JH flows into five types, which will be discussed in more detail below, and suggested that they might be used to locally approximate the flow in channels with walls of sufficiently small curvature, noting that this would not require the channel to be symmetric. However, in a more general study of bifurcations in channel flow, Sobey and Drazin (1986) suggested that JH flows which were not uni-directional, i.e. pure outflow, were unstable, and hence that JH flow would not approximate flow in a channel when there was no appropriate JH flow with radial velocity of only one sign (for any value of α (Re) there is a maximum value of Re (α), Re_2 (α_2), for which pure outflow can exist).

Banks *et al.* (1988) considered a range of perturbations of JH flow, using both linear and weakly non-linear theory. They found that symmetric JH flows are unstable spatially unless they are uni-directional, and hence that the local approximation suggested by Fraenkel is useful only under limited conditions, in agreement with Sobey & Drazin. Banks *et al.* also found, considering both spatial and temporal stability of the flow, that in appropriate circumstances the exact form of the upstream and downstream conditions can have a significant effect on the flow.

As JH flows have two independent parameters, α and Re, it is not possible to make a detailed investigation of the entire parameter space, if for no other reason, because

of the unrealistically large computational effort this would require. We have chosen to concentrate on Reynolds numbers of $O(10^2)$ close to the region (i.e. values of α) where uni-directional flow is no longer possible, and the basic JH flow has been predicted to be unstable. Reynolds numbers of this magnitude were chosen to be consistent with previous studies of flow in non-uniform channels which have shown the rich and complex structure of the flow patterns, particularly for unsteady flow where a strong 'vortex wave' is commonly found, see e.g. Sobey (1985), Pedley & Stephanoff (1985), Tutty (1992) and Tutty & Pedley (1993). Steady flow in such channels, which have parallel walls for the most part, is usually much less interesting, with a relatively weak wave which decays rapidly downstream, see e.g. Armaly *et al.* (1993). However, as will be seen below, relatively small changes to the channel geometry can generate large changes in steady flow patterns, so that they resemble previously reported unsteady flows rather than the usual steady flow. Also, the parameter range chosen enables us to investigate the predictions of Sobey & Drazin (1986) and Banks *et al.* (1988) concerning the spatial stability of JH flow, and the applicability of these results to flow in non-uniform channels. In most aspects our results support their predictions. Of particular interest here is the prediction by Sobey & Drazin (1986) that the critical bifurcation leads to subcritical instability. In contrast, in a non-linear analysis of JH flow in a finite-length channel, Hamadiche, Scott & Jeandel (1994) found that the loss of stability is supercritical. We have found solutions with a large-amplitude, constant-strength wave in the non-parallel section of the channel, rather than JH flow, for both symmetric and asymmetric channels in regions of the (Re, α) parameter space for which stable symmetric JH flows exist. We interpret these results as strongly supporting the hypothesis of Sobey & Drazin (1986), i.e. that JH flow becomes unstable subcritically.

We note here that the references to 'stability' in this paper are not concerned with the development of perturbations to the flow in time, as is usual, but the spatial behaviour of steady flows. In particular, a flow is described as unstable if the flow far down the channel is not one of the possible JH flows.

The formulation of the problem is given in §2, along with a brief discussion of the numerical method. Relevant aspects of JH flow are considered in §3, and the main results in §4, followed by a discussion of these results in §5.

2. Formulation

The channel used for most of the calculations reported below has an expansion in the form of a step in the upper wall at $x^* = 0$ with a change from a dimensional width of $2a^*$ to $(2 + \epsilon)a^*$, where ϵ may be zero, followed by a gradual change in width for $x^* > 0$ with the upper wall at an angle of 2α to the lower wall, which is undisturbed, with a further change back to parallel walls at $x^* = La^*$ (figure 1). The reversion to a parallel channel downstream of the step was adopted both to simplify the application of downstream boundary conditions in the numerical method and to produce a physically sensible problem when α is negative, while the angle was taken as 2α rather than α to be consistent with the usual formulation for JH flows. The geometry for a symmetric channel is obtained by reflection about the lower wall in figure 1, rescaled so that the channel still has width $2a^*$ upstream, and a change in slope of α on each wall. The coordinates are non-dimensionalized on (half) the upstream channel width so that $(x, y) = (x^*, y^*)/a^*$. The corresponding velocity components are $U_0^*(u, v)$ where the reference velocity is $U_0^* = Q^*/2a^*$ and Q^* is the volumetric flow rate.

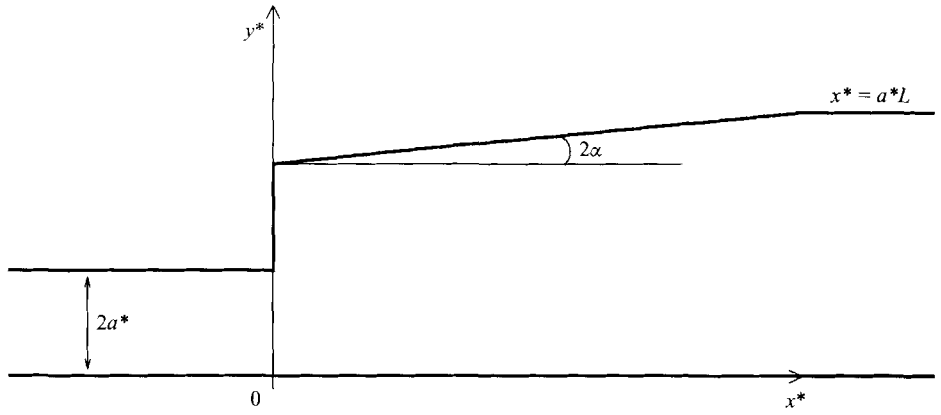

FIGURE 1. Channel geometry (not to scale).

The Reynolds number Re is defined by

$$Re = Q^*/2\nu \tag{2.1}$$

where ν is the kinematic viscosity. For steady flow the vorticity transport equation becomes

$$u\frac{\partial\zeta}{\partial x} + v\frac{\partial\zeta}{\partial y} = \frac{1}{Re}\nabla^2\zeta, \tag{2.2}$$

where, as usual,

$$\zeta = -\nabla^2\psi \tag{2.3}$$

and

$$(u, v) = \left(\frac{\partial\psi}{\partial y}, -\frac{\partial\psi}{\partial x}\right). \tag{2.4}$$

The boundary conditions are the usual no slip and zero normal velocity on the walls,

$$\psi = \frac{\partial\psi}{\partial y} = 0 \text{ on } y = 0 \text{ and } \psi = 2, \quad \frac{\partial\psi}{\partial n} = 0 \text{ on } y = y_w, \tag{2.5}$$

where n denotes the normal to the upper wall, and

$$y_w = \begin{cases} 2, & x < 0 \\ y, & x = 0, \quad 2 < y < 2 + \epsilon \\ 2 + \epsilon + x\tan 2\alpha, & 0 < x < L \\ 2 + \epsilon + L\tan 2\alpha, & x > L \end{cases} \tag{2.6}$$

gives the position of the upper wall, and parallel flow upstream and downstream, i.e.

$$\frac{\partial^m\psi}{\partial x^m} \to 0, \frac{\partial^m\zeta}{\partial x^m} \to 0 \text{ as } x \to \pm\infty, \tag{2.7}$$

where $m \geqslant 1$. In practice Poiseuille flow is imposed at the inlet, and (2.7) with $m = 2$ at the outlet.

To solve the problem defined by (2.2)–(2.7), first we map the non-uniform channel onto a uniform channel of unit width using a combination of an exponential transform which maps the uniform channel to a half-plane, followed by a Schwarz–Christoffel

transform which maps the half-plane to the physical channel, i.e.

$$\frac{\mathrm{d}z}{\mathrm{d}Z} = 2(1-\mathrm{e}^{\pi(z-a)})^{1/2}(1-\mathrm{e}^{\pi(z-b)})^{-1/2+2\alpha/\pi}(1-\mathrm{e}^{\pi(z-c)})^{-2\alpha/\pi} \tag{2.8}$$

where $z = x + \mathrm{i}y$ and $Z = X + \mathrm{i}Y$. The corners $(x, y) = (0, 2)$, $(0, 2+\epsilon)$ and $(L, 2+\epsilon+L\tan 2\alpha)$ in physical space map to $Z = a$, b and c respectively in the computational space, with $\mathrm{Im}(a)=\mathrm{Im}(b)=\mathrm{Im}(c)=1$, so that the computational space is $0 \leqslant X \leqslant X_{max}$, $0 \leqslant Y \leqslant 1$.

With this mapping, the vorticity transport equation and the Poisson equation (2.2) and (2.3) become

$$U\frac{\partial\zeta}{\partial X} + V\frac{\partial\zeta}{\partial Y} = \frac{1}{Re}\nabla^2\zeta, \tag{2.9}$$

and

$$J\zeta = -\nabla^2\psi \tag{2.10}$$

respectively, where $J = |\mathrm{d}z/\mathrm{d}Z|^2$, ∇^2 is now the Laplacian in computational space, and

$$(U, V) = \left(\frac{\partial\psi}{\partial Y}, -\frac{\partial\psi}{\partial X}\right). \tag{2.11}$$

The outflow boundary conditions now become $\partial^2\psi/\partial X^2 = \partial^2\zeta/\partial X^2 = 0$ at $X = X_{max}$.

The computational grid used was a uniform rectangular grid in (X, Y). A fourth-order finite difference scheme was used to solve (2.9)–(2.11) on this grid. This scheme is a straightforward steady version of the unsteady method used by Tutty & Pedley (1993), and details can be found there. For most of the detailed results below, 48 grid steps were used across the channel (this was previously found to be suitable for flows of the type considered in this study). The accuracy and behaviour of the numerical procedure is discussed below after the results have been presented.

Note that, if the channel does not revert to a parallel-sided channel at $x = L$, then the final term in (2.8) should be dropped (equivalently, let $\mathrm{Re}(c)\to\infty$ in (2.8)). This gives

$$\frac{\mathrm{d}z}{\mathrm{d}Z} \to K\mathrm{e}^{2\alpha Z} \quad \text{and} \quad J \to K^2\mathrm{e}^{4\alpha X} \quad \text{as} \quad X \to \infty \tag{2.12}$$

where $K = 2\exp(\frac{1}{2}\pi(b-a) - 2\alpha(b-\mathrm{i}))$ is a positive real constant.

3. Jeffery–Hamel flow

Details of JH flow can be found in many references (e.g. Fraenkel 1962; Banks *et al.* 1988); here we consider only the aspects that are relevant to the current study. The standard geometry and coordinate system for JH flow are shown in figure 2(*a*). The (dimensional) streamfunction can be written as $\psi^*(r^*, \theta) = \frac{1}{2}Q^*G(\eta, \alpha, Re)$, where $Re = Q^*/2\nu$ as before, $\eta = \theta/\alpha$, and (r^*, θ) are polar coordinates. The Navier–Stokes equations now reduce to

$$G_{\eta\eta\eta\eta} + 4\alpha^2 G_{\eta\eta} + 2\alpha Re G_\eta G_{\eta\eta} = 0 \tag{3.1}$$

and the boundary conditions are

$$G = \pm 1 \quad \text{and} \quad G_\eta = 0 \quad \text{at} \quad \eta = \pm 1. \tag{3.2}$$

Fraenkel (1962) classified the solutions of (3.1) and (3.2) into five types, I–V. Types I and II_1 have pure symmetric outflow, and type III_1 pure symmetric inflow. Types

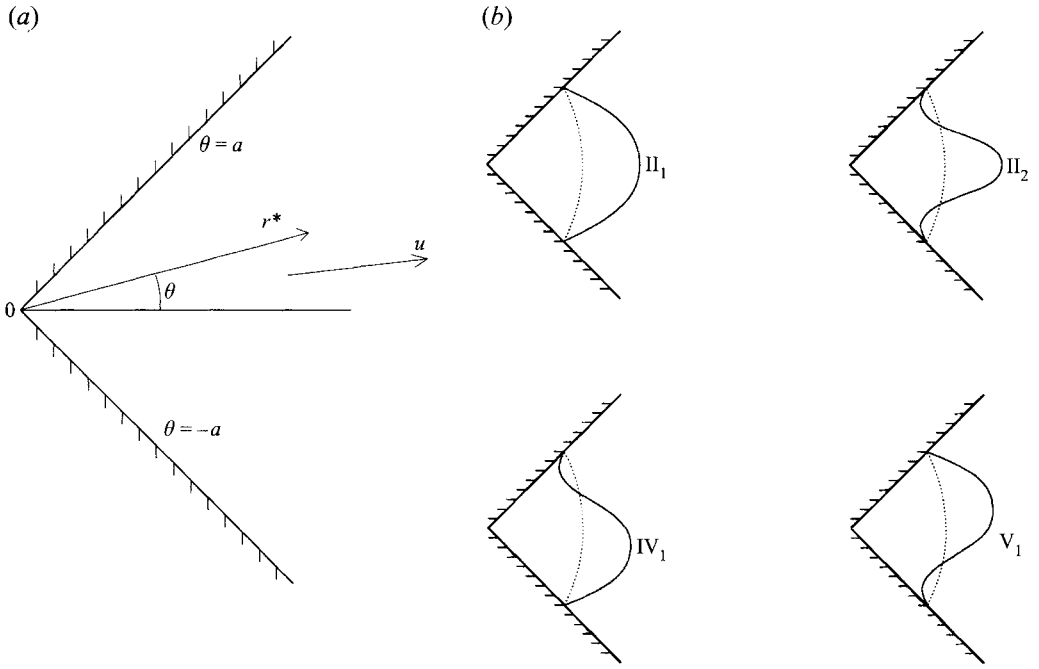

FIGURE 2. Geometry for Jeffery–Hamel flow (*a*) and basic Jeffery–Hamel flows (*b*).

II_n and III_n ($n > 1$) are symmetric but with regions of inflow and outflow, and $2n-2$ zeros in the radial velocity. Types IV_n and V_n are asymmetric with regions of inflow and outflow with $2n-1$ zeros. Types IV_n have outflow adjacent to the lower wall (and by implication inflow at the upper wall), while any V_n is the mirror image of a IV_n. Velocity profiles for the basic JH flows are shown schematically in figure 2(*b*). For any pair of values of the parameters, α and Re, there are many possible JH flows. However, Fraenkel imposed a further condition which led to uniqueness in a limited region of the (Re, α)-space, with analytic continuation between the types of solution in this region. Also, Fraenkel mapped the boundaries between the various types of solution, as shown in figure 3, which includes both Fraenkel's results and extensions of them from Buitrago (1983).

For this study, the most important boundaries in figure 3 are $\mathscr{B}_2$ and $\mathscr{B}_3$, denoted by (Re_2, α_2) and (Re_3, α_3) respectively (the other boundaries are shown for completeness). On $\mathscr{B}_2$, where the wall shear is zero ($G_{\eta\eta}(\pm 1) = 0$), flows of types II_1, II_2, IV_1 and V_2 coincide. Below $\mathscr{B}_2$ pure symmetric outflow (type I or II_1) is possible, and is the appropriate unique solution in Fraenkel's formulation, while above $\mathscr{B}_2$ uni-directional flow cannot occur, and all solutions must have regions of inflow and outflow. Sobey & Drazin (1986) recognized that a subcritical pitchfork bifurcation occurs on $\mathscr{B}_2$, with II_1 stable subcritically (below $\mathscr{B}_2$), II_2 unstable supercritically (above $\mathscr{B}_2$), and IV_1 and V_1 unstable subcritically. This led Sobey & Drazin to question whether JH flows could be used to approximate flow in a channel with walls of small curvature when there was no uni-directional JH flow.

Banks *et al.* (1988) studied the spatial development of arbitrary small steady two-dimensional perturbations of JH flow, using both linear and weakly non-linear theory. They found that type I and II_1 flow were stable, and hence that symmetric JH flow could be used to approximate flow in a channel below $\mathscr{B}_2$, but not above where

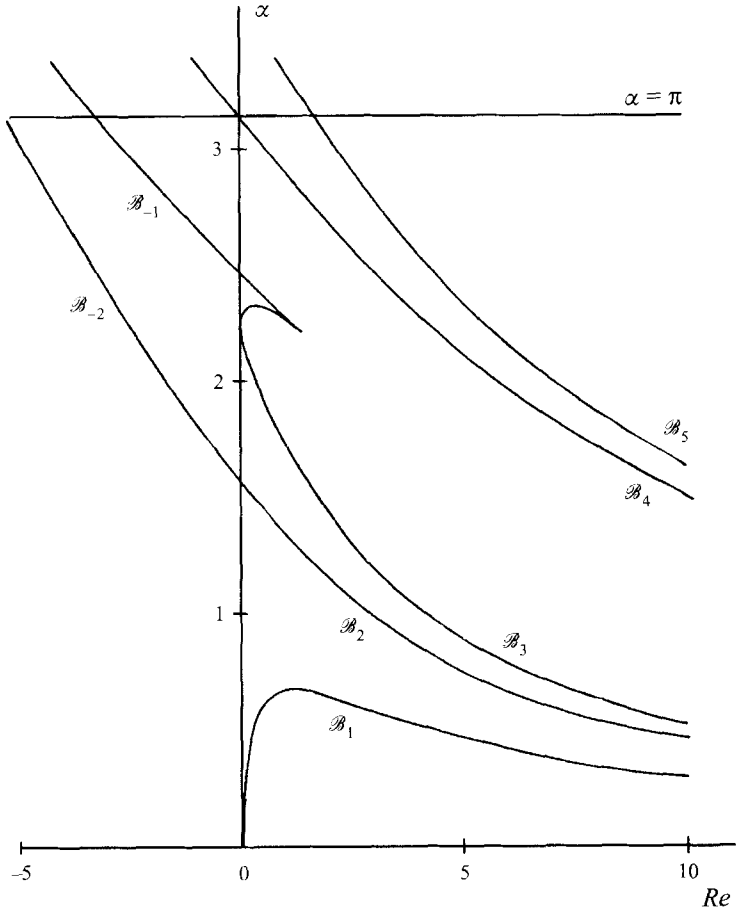

FIGURE 3. Critical boundaries of Jeffery–Hamel flow in the (Re, α)-plane.

Π_2 is unstable. Also, Banks *et al.* suggested that, in a channel in which the angle between the walls varies, provided that $\alpha(x)$ does not exceed $\alpha_2(Re)$ by too much or for too far downstream then the disturbances will ultimately decay downstream where $\alpha(x) < \alpha_2(Re)$, and hence that JH flow may still be useful in such conditions. As we will see below, for our problem the upstream conditions play a crucial role in whether JH flow is re-established, consistent with the importance of the upstream conditions found by Banks *et al.*. In contrast, we find that the downstream conditions have a strictly local effect.

For $\mathscr{B}_3$, Fraenkel showed that there is a singularity such that there is no continuation of the Π_2 flow as $\mathscr{B}_3$ is crossed from below, i.e. we have $\partial G/\partial\alpha \to \infty$ as $\alpha \to \alpha_3(Re)$, or equivalently, $\partial G/\partial Re \to \infty$ as $Re \to Re_3(\alpha)$. To be more precise, fixing α and varying Re, the wall shear behaves as

$$G_{yy}(0, Re) = G_{yy}(0, Re_3) + \bar{K}(Re_3 - Re)^{1/2} + \ldots \quad \text{as} \quad Re \to Re_3-, \tag{3.3}$$

where $\bar{K}$ is a positive constant.

Asymptotically

$$Re_2 \sim 4.712\alpha^{-1} \quad \text{and} \quad Re_3 \sim 5.461\alpha^{-1} \quad \text{for} \quad Re \gg 1 \tag{3.4}$$

(Fraenkel 1962). Further details of $\mathscr{B}_2$ and $\mathscr{B}_3$ can be found in the tables given in Fraenkel (1962) or of $\mathscr{B}_2$ in Sobey & Drazin (1988).

The description of JH flows given above, which is based on Fraenkel's (1962) classification, is consistent, but does not take full account of the detail and complexity of JH flows, particularly with respect to the multiple solutions. Using Newton's method with a second-order finite difference scheme, the behaviour of JH flow near $\mathscr{B}_2$ has been investigated. To be consistent with the Navier–Stokes problems considered below, we take $\alpha = 2°$, which gives $Re_2 \approx 135$ from (3.4). Starting with a sufficiently low Re (< 50) there was no difficulty in generating the II_1 flow, and, by increasing Re, moving smoothly through $\mathscr{B}_2$ to obtain the II_2 solution which terminated at $\mathscr{B}_3$. However, IV_1 and V_1 solutions were also found for $Re < Re_2$, and by increasing Re gradually they were tracked to the subcritical pitchfork bifurcation where types II_1, II_2, IV_1 and V_1 coincide. By decreasing or increasing Re, we could then follow the II_1 or II_2 flow, respectively, but not move directly back to the IV_1 or V_1 flow used to approach the bifurcation. Note that although there is no continuation of the II_2 solution as the $\mathscr{B}_3$ boundary is crossed from below, this solution does not terminate at $\mathscr{B}_3$. Rather there is a fold in the solution surface (see e.g. Banks *et al.*, figure 4), and for Re close to but below Re_3 there are two II_2 solutions, the second with larger shear rates near the wall and $\bar{K}$ negative in (3.3). This second II_2 mode was tracked back to an Re value below one with wall shear rates of $O(10^4)$. A number of other branches of the solution surface involving more complex JH flows were tracked in a similar manner.

Three different coordinate systems have been introduced: physical (x, y), computational (X, Y), and for pure JH flow (r^*, θ). There is however a direct connection between the last two away from the corners of the channel shown in figure 1. When (2.12) holds

$$\theta = \alpha(2Y - 1), \quad \text{i.e.} \quad \eta = 2Y - 1, \quad \text{and} \quad r^* \propto 2a^* \mathrm{e}^{2\alpha X}. \tag{3.5}$$

As will be seen below, away from the corners the computational coordinates are the natural coordinate system in which to view the non-linear development of the flow.

4. Navier–Stokes flow

The Navier–Stokes problem defined above has four independent parameters: α, Re, ϵ, and L. Investigating the full parameter space would be a formidable task. Fortunately, the results discussed above, in particular those of Sobey & Drazin (1986) and Banks *et al.* (1988), suggest that the most interesting results will be near or above the $\mathscr{B}_2$ boundary. In addition we will concentrate on channels in which α is small and where $Re_2 = O(100)$, both to compare the results with unsteady flows in non-uniform channels at these Re, and because the results may be relevant to experimental situations where normal tolerances in producing apparatus may lead to channels with slightly non-parallel walls.

As is well known from previous studies of steady flow in a channel with a step expansion but otherwise parallel walls (e.g. Armaly *et al.* 1983; Sobey 1985), at Reynolds numbers of $O(100)$ a weak standing wave is generated downstream of the step, with one or more eddies, the largest and strongest of which is in the lee of the step. Compared with the waves which can be generated with unsteady flow in the same channel at the same Reynolds number, the steady wave has a much longer wavelength, and has fewer, weaker eddies.

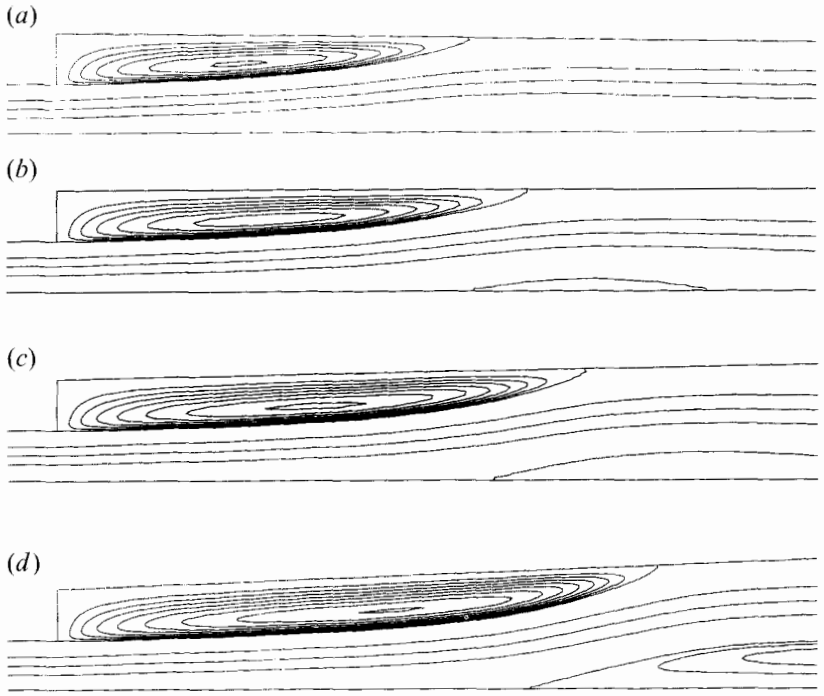

FIGURE 4. Streamlines near the expansion for $Re = 125$, $\epsilon = 2$, and (a–d), $\alpha = -\frac{1}{2}°$, 0°, $\frac{1}{2}°$, and 1°. $-2 \leqslant x \leqslant 30$.

Figure 4 shows streamlines for flow in a channel in which the width doubles at $x = 0$ ($\epsilon = 2$) for $Re = 125$ and $\alpha = -\frac{1}{2}°$, 0°, $\frac{1}{2}°$, and 1°. The channel reverts to parallel further downstream but the details do not significantly affect the flow in the region shown in figure 4. For all these flows $Re < Re_2(\alpha)$, and in general the flow resembles that shown in previous studies: the main eddy is well developed, and when the walls are parallel ($\alpha = 0°$) there is also a small, very weak second eddy on the lower wall downstream of the main eddy. The second eddy does not exist when the upper wall has a small negative slope (figure 4a, $\alpha = -\frac{1}{2}°$), but both its length and strength increase rapidly when the upper wall takes a small positive slope (figure 4c, d). However, even for $\alpha = 1°$, when the second eddy extends from $x = 18.4$ to $x = 56.6$ there is no sign of a third eddy. Also, figure 4 shows that both the length and (from the number of streamlines plotted) the strength of the main eddy increase as α increases. In fact, as can be seen from figure 5, the increase in length with α is slightly greater than linear. For these cases, examination of the solutions showed that, downstream of the weak wave generated by the step but before the walls of the channel became parallel again, type II_1 JH flow occurred, as expected.

A similar set of calculations to those shown in figure 4 were performed for $Re = 62.5$. Similar behaviour was found, although the wave is much weaker such that even for $\alpha = 1°$ there was no sign of a second eddy. As expected, the primary eddy is shorter and weaker than with $Re = 125$, but again it increases in length slightly faster than linearly with α.

For $\alpha = 2°$, $Re = 125 < Re_2$, and again we might expect a weak wave with JH flow downstream of it. (For the moment assume that the channel does not change shape far downstream and hence that the walls are non-parallel at the outlet –

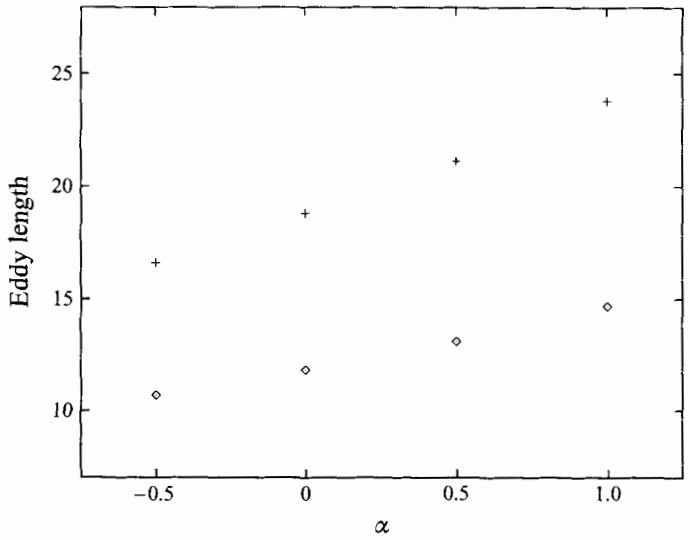

FIGURE 5. Eddy length against α for $\epsilon = 2$ and: $\diamond$, $Re = 62.5$; + $Re = 125$.

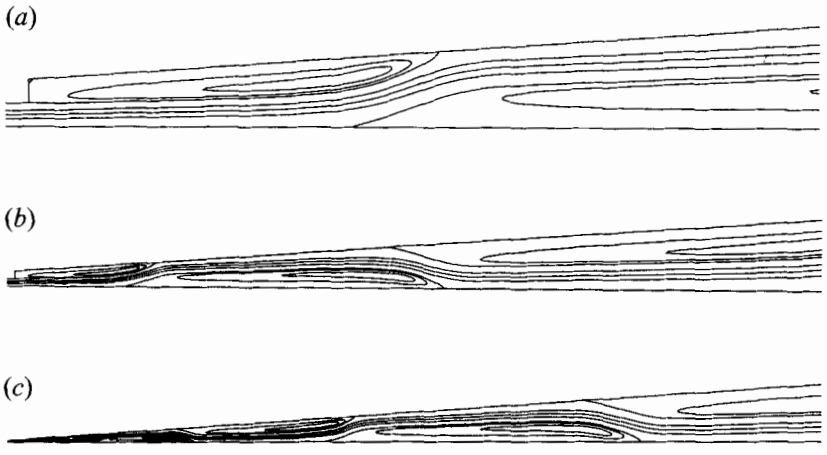

FIGURE 6. Streamlines near the expansion for $Re = 125$, $\alpha = 2°$, $\epsilon = 2$, and (a) $-2 \leqslant x \leqslant 67$, ($b$) $-2 \leqslant x \leqslant 200$, and ($c$) $-2 \leqslant x \leqslant 2000$.

this will be discussed further below.) Figure 6 shows the streamlines for $\alpha = 2°$, $Re = 125$ and $\epsilon = 2$. In figure 6(a), as expected, there is an eddy in the lee of the step which is both stronger and longer than that shown in figure 4(d) with a much larger second eddy on the lower wall. However by replotting for larger ranges of x (figure 6b, c) we see that there is a sequence of eddies alternating on the upper and lower walls extending much further downstream. The streamlines for this case are plotted against the computational coordinates in figure 7(a), which shows a regular wave extending very far downstream (this calculation had $X_{max} = 300$ which corresponds to $x \approx 3.5 \times 10^{10}$). From figure 7($a$), the wave appears to have a constant wavelength and strength in computational space along virtually the entire channel. Detailed examination of the solution shows that this is indeed the case: figure 7(b) shows the streamlines for a section of the channel where successive flow structures

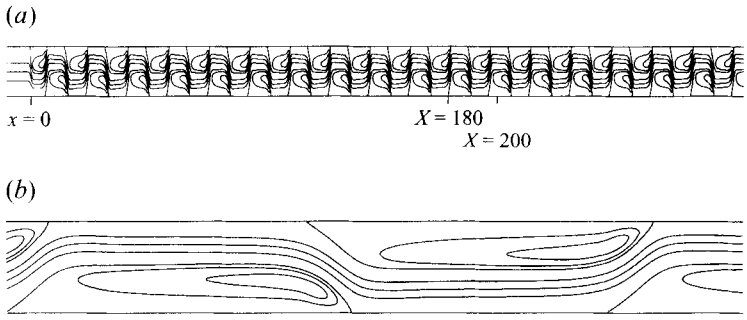

FIGURE 7. Streamlines in computational space for $Re = 125$, $\alpha = 2^{\circ}$, and $\epsilon = 2$. (*a*) $0 \leqslant X \leqslant 300$, (*b*) $180 \leqslant X \leqslant 200$.

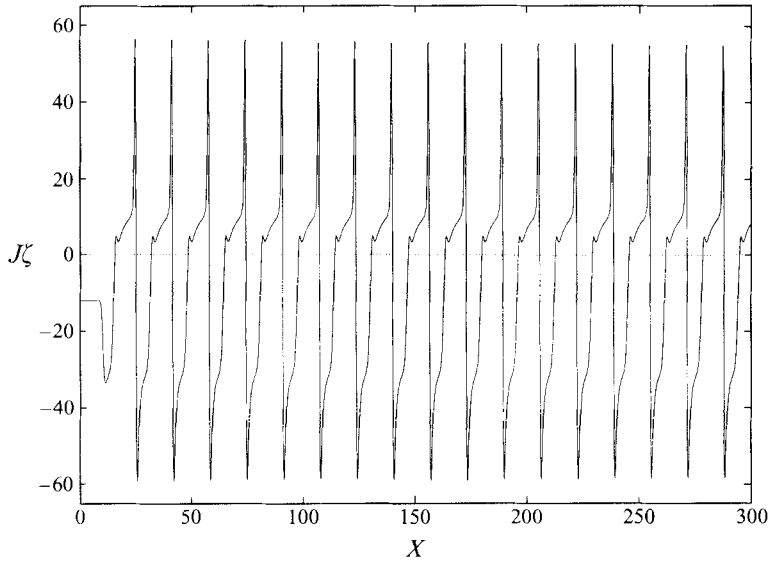

FIGURE 8. Lower-wall vorticity in computational space: $J\zeta$ against X for $Re = 125$, $\alpha = 2^{o}$, and $\epsilon = 2$. $0 \leqslant X \leqslant 300$.

are graphically indistinguishable. Also, from (2.10) we see that if ψ has a regular pattern in computational space, then so should $J\zeta$. Figure 8 shows $J\zeta$ against X for the lower (straight) wall. This confirms the pattern of figure 7, with a wave that is essentially uniform along the channel downstream of the step.

For this geometry $Re = 150$ lies between $\mathscr{B}_2$ and $\mathscr{B}_3$, and, in contrast to the case with $Re = 125$, JH flow might not be expected downstream of the step. Figure 9 displays the streamlines in computational space. This shows a similar pattern to that of figure 7 for $Re = 125$, with a regular wave extending far downstream. The wave is clearly more complex than for $Re = 125$: the eddies have multiple cores and there are regions of secondary separation on the walls, as shown in figure 9(*b*). However, the wave now develops gradually, and approaches its final form asymptotically with X, as can be seen in figure 9(*a*) and figure 10, which displays $J\zeta$ against X for the lower wall. Close examination of the solution shows that the wave does not reach its final state until X is greater than 100 (see also figure 12). The wave is much stronger for

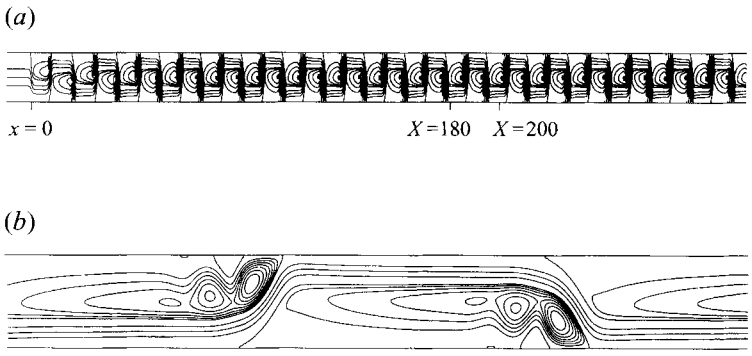

FIGURE 9. Streamlines in computational space for $Re = 150$, $\alpha = 2°$, and $\epsilon = 2$. (*a*) $0 \leqslant X \leqslant 300$, (*b*) $180 \leqslant X \leqslant 200$.

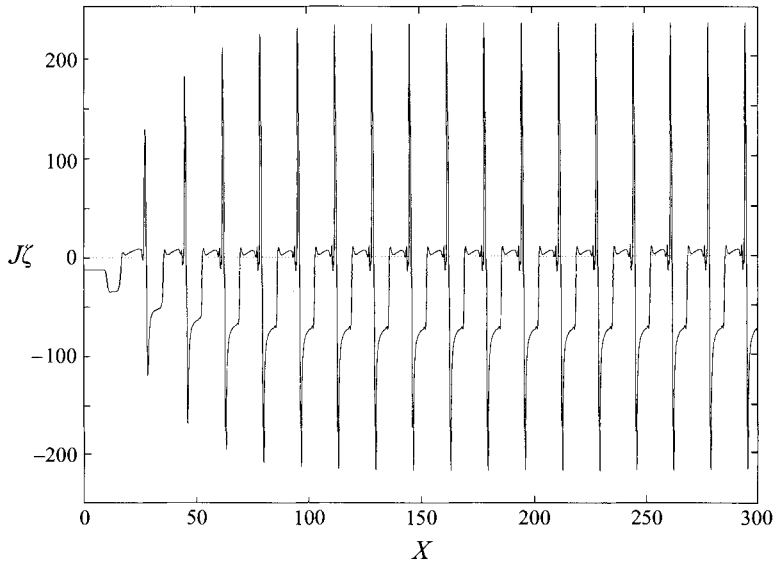

FIGURE 10. Lower-wall vorticity in computational space: $J\zeta$ against X for $Re = 150$, $\alpha = 2°$, and $\epsilon = 2$. $0 \leqslant X \leqslant 300$.

$Re = 150$ than for $Re = 125$, with much larger peak values of the wall shear stress, as can be seen from figures 8 and 10.

It is easily shown that a constant wavelength in computational space implies a linear variation in the wavelength with x in physical space. In figure 11 the eddy length, calculated from the values of x at which $\psi = 1$ at the (computational) centre of the channel, which gives approximately half the wavelength, has been plotted against x for $Re = 125$ and 150. Both data sets appear to fall exactly on a straight line. This, however, is deceptive near the step, where the details in figure 11 are lost due to the scale. As an alternative, the eddy length divided by the position of the eddy in physical space has been plotted in figure 12. As expected, both lines tend to a constant for large X, and they clearly show the relative decrease in the wavelength away from the step. There is little difference in the wavelength for these two values of Re. The eddy strength can be measured by calculating the maximum difference of the streamfunction in an eddy from that on the of the wall to which the eddy is

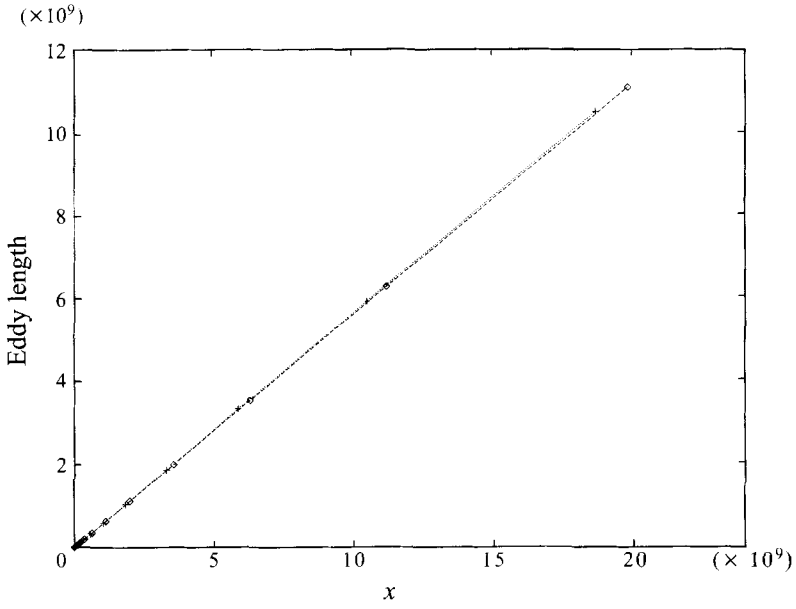

FIGURE 11. Eddy length against x for $\alpha = 2°$, $\epsilon = 2$, and: ◇, $Re = 125$; +, $Re = 150$.

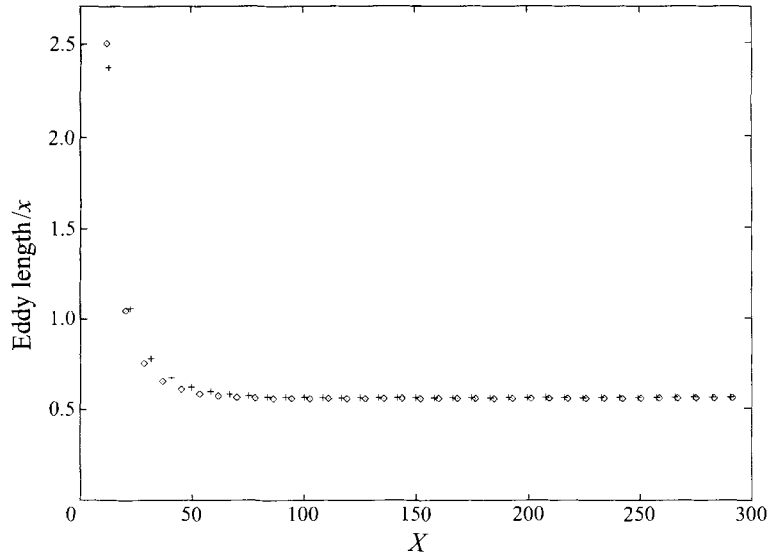

FIGURE 12. Eddy length over position (x) against X for $\alpha = 2°$, $\epsilon = 2$, and: ◇, $Re = 125$; +, $Re = 150$.

attached. This is shown in figure 13, and it can be seen that the eddies are much stronger for $Re = 150$ than 125, and that for the smaller value of Re the wave has constant strength almost immediately downstream of the step, while for $Re = 150$ it asymptotes to constant strength for $X > 100$, consistent with the behaviour of the wall shear stress (figure 10).

The step size was varied between zero and 2 for both $Re = 125$ and $Re = 150$. For $Re = 125$ and $\epsilon = 1$, the extended wave did not occur, and the flow was similar

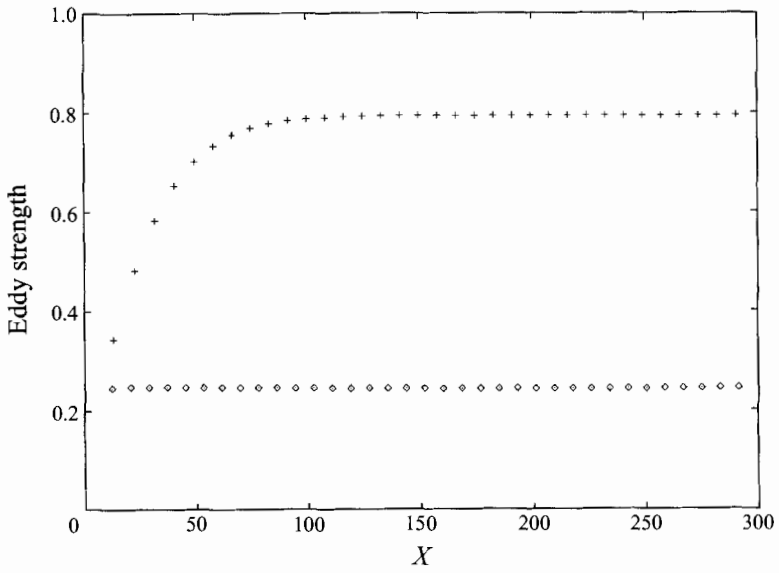

FIGURE 13. Eddy strength against X for $\alpha = 2°$, $\epsilon = 2$, and: $\diamond$, $Re = 125$; $+$, $Re = 150$.

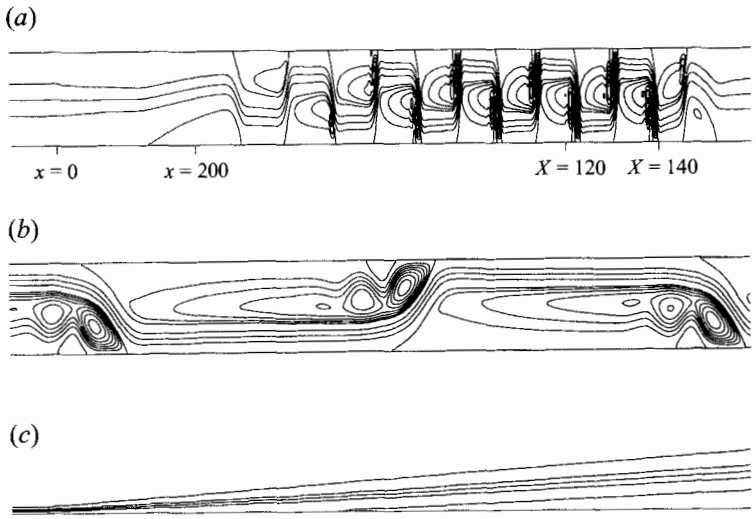

FIGURE 14. Streamlines for $Re = 150$, $\alpha = 2°$, and $\epsilon = 0$. (a) Computational space: $0 \leqslant X \leqslant 160$, ($b$) computational space: $120 \leqslant X \leqslant 140$, ($c$) physical space: $-10 \leqslant x \leqslant 200$.

to that shown in figure 4 with a limited disturbance generated by the step and JH flow downstream. For $Re = 150$, a wave was generated both for $\epsilon = 1$ and zero. For the latter case figure 14(a) shows streamlines in computational space for the entire channel, figure 14(b) details in computational space near the outlet, and figure 14(c) in physical space near the change in geometry. Clearly, the wave will eventually take the same form as shown in figure 9 for $\epsilon = 2$, but it takes longer to develop, and close to the change in shape of the upper wall at $x = 0$ there is a gradual evolution of the flow with a long separation bubble formed on the lower wall. Also, in this channel $X_{max} = 160$ and a second corner was included at $X = 140$ so that the walls were

parallel again for $X > 140$. It can be seen from figures 14(*a*) and 14(*b*) that there is very limited upstream influence from this change in geometry (this was found also in other runs), and that the wave decays quickly once the walls become parallel again, with Poiseuille flow re-established downstream of this corner. A detailed examination of the solution for $\epsilon = 0$ showed that the flow is not quite fully developed when the channel walls revert to parallel at $X = 140$ (small differences can be seen in the flow structures shown in figures 9*b* and 14*b*). This is not surprising given the geometry and the way the wave asymptotes to its final form for this Reynolds number when $\epsilon = 2$. However, calculations were also performed on a longer channel with $\epsilon = 0$, but with a grid step of 1/32 rather than 1/48 (to save computational effort), and in this case it was found that the final form of the wave was identical to that for $\epsilon = 2$ with this grid step (the dependence of the solution on the grid step is discussed below).

A set of calculations was performed for a symmetric channel with no step, i.e. both walls changed shape at $x = 0$ so that they had a 2° slope for $x > 0$. For $Re = 150$ an extended wave was generated, with symmetry breaking near the change in geometry so that the first eddy was formed (arbitrarily) on the upper wall. In addition, in this case a symmetric solution which tended to II_2 JH flow far downstream was obtained by explicitly forcing symmetry. Also, a number of calculations were performed for Re close to Re_2 with $\epsilon = 0$, both for symmetric and asymmetric channels. No wave was found for $Re < Re_2 \approx 135$, even with $Re = 134.5$ when the channel was asymmetric and a converged solution with a fully developed wave obtained with a higher Re was used as the initial approximation to the solution. For $Re = 135.5$, which is just above Re_2, a wave was found for the asymmetric channel, although even with $X_{max} = 300$ the wave developed very slowly with relatively few eddies. For the symmetric channel, again there was symmetry breaking, with an asymmetric disturbance growing slowly downstream of the change in geometry, eventually developing into a full non-linear wave.

A further set of calculations was performed for a symmetric channel with a 2° slope on each wall, but with a step on each wall so that the channel doubled in width at $x = 0$. For $Re = 120$, there was symmetry breaking near the steps, as would be expected from the results for stepped channels with parallel walls (see e.g. Sobey 1985), but the wave decayed downstream with the flow tending asymptotically to II_1 JH flow. In contrast, for $Re = 125$, which is still less than Re_2, an extended wave of constant strength, similar to that shown in figures 6–8, was generated. Again, multiple solutions were found: a symmetric solution, generated by forcing symmetry, was converged to machine precision and was then used as the starting condition for a run in which the full channel was considered, leading to the solution with the extended wave. Note that in this case the perturbations to the symmetric flow which excite the instability must arise from the rounding errors inherent in the arithmetic procedure.

A large number of runs were performed during this study. A summary of the more important results is given in table 1. The apparently anomalous results are those for $\alpha = 5.73°$, $Re = 45$ and $\epsilon = 2$, and the different cases with $\alpha = 2°$, $Re = 125$ and $\epsilon = 2$, where waves were found although these points are below $\mathscr{B}_2$ in the (Re, α) parameter space. These results demonstrate that near $\mathscr{B}_2$ the generation/existence of a wave depends on the upstream conditions as well as on the values of Re and α, which is consistent with the predictions of Banks *et al.* (1988). It is also consistent with the prediction of Sobey & Drazin (1986) that the bifurcation at $\mathscr{B}_2$ leads to a subcritical instability.

α (deg.)	Re	ϵ	$Re > Re_2(\alpha)$	Wave
1	125	2	No	No
2	120	2	No	No
2	125	2	No	Yes
2	150	2	Yes	Yes
2	125	1	No	No
2	125	0	No	No
2	134.5	0	No	No
2	135.5	0	Yes	Yes
2	150	0	Yes	Yes
1	300	2	Yes	Yes
5.73	45	2	No	Yes
5.73	50	2	Yes	Yes

TABLE 1. Summary of results. The entries for $\alpha = 2°$, $\epsilon = 0$ and $Re = 134.5$, 135.5 and 150, and $\alpha = 2°$, $\epsilon = 2$ and $Re = 120$ and 125 cover both asymmetric and symmetric cases.

Finally in this section, we wish to discuss the effect of some details of the numerical procedure on the results. The problem was defined in §2 with the channel walls reverting to parallel far downstream. However, in many of the calculations the downstream conditions $\partial^2\psi/\partial X^2 = \partial^2\zeta/\partial X^2 = 0$ could be applied at the downstream boundary with non-parallel walls with very little effect on the solution except immediately adjacent to the boundary. For example, in figures 6–8 the walls are non-parallel at the outlet, but e.g. in figure 7(*a*) there is no noticeable effect of the downstream boundary condition on flow structures near the outlet. Where possible, non-parallel walls were used to the end of the computational domain. An exception was when ϵ was zero, e.g. as in figure 14, when difficulties were encountered in converging the iterative procedure unless L was less than X_{max}. Another, more significant, point concerns the convergence criterion used when calculating flow patterns near a bifurcation. Usually, with the code employed in this study, convergence is tested using the L_∞ norm with the streamfunction, i.e.

$$\max_{j,k} \mid \psi_{j,k}^{(m+1)} - \psi_{j,k}^{(m)} \mid < \text{tol} \tag{4.1}$$

where m is the iteration count and j and k are the grid indices. However, the use of this convergence test with any fixed value of tol was potentially highly deceptive. For example, for the calculation for a symmetric channel with $\epsilon = 0$, $\alpha = 2°$ (on each wall) and $Re = 150$, the norm in (4.1) decayed to less than 2×10^{-15}, close to the machine precision of $O(10^{-16})$, with an apparently symmetric solution, before the norm started to grow again as the wave was generated. However, examination of the solution when the iterative process was terminated using (4.1) with tol = 10^{-14}, showed that although the flow far downstream of the change in shape was very close to a II_2 JH flow with the streamfunction largely independent of the (radial) distance along the channel, there was a very weak but definite oscillatory disturbance superposed on this solution. This disturbance grew slowly as the iterations proceeded beyond this stage, until eventually the full non-linear disturbance was generated. The initial disturbance was most noticeable along the centreline where there was a fluctuation in $J\zeta$ of $O(10^{-10})$. In contrast, for some cases with non-parallel walls extending to the downstream boundary, the change in ψ as measured by (4.1) did not decay below $O(10^{-8})$ due to the effects of the downstream boundary condition, although it was clear that the solution had in fact converged. For this reason, detailed examination

of the 'dynamic' behaviour of the solution as the iterations continued, as well as the size and behaviour of the L_∞ measures of the change in the streamfunction and the vorticity, were used to determine convergence rather than a single formal test. In particular, if the flow is stable and a JH flow exists, the behaviour of the solution along the (numerical) centreline was a sensitive indicator of convergence: for a symmetric solution the scaled vorticity $J\zeta$ should be close to zero, while it should tend to zero asymptotically for an asymmetric solution. In contrast, the presence of a growing (oscillatory) disturbance along the centreline indicates an unstable flow. If the flow is unstable and a wave develops, then the change in vorticity on the walls can be used to monitor the final convergence of the numerical process. As well as the change in ψ and ζ, the residuals for the discrete form of the governing equations, (2.9) and (2.10), were calculated using an L_2 norm. The behaviour of the residuals closely followed that of the L_∞ norm for the streamfunction, and showed that in all cases the finite difference equations were satisfied to a very fine tolerance.

The results presented in detail above (figures 6–14) are with a square grid with a step of $h = 1/48$, while (some of) the others referred to in table 1 were for $h = 1/32$. A number of runs were performed to check the accuracy of the results presented: in particular, for $Re = 150$, $\alpha = 2°$, and $\epsilon = 2$, runs were performed with 1/16, 1/24, 1/32, 1/40 and 1/48. An extended wave was generated in all cases, and comparison of the streamline patterns and the wall shear stress for these runs showed that there would be no substantial change in the solution with a finer grid, although there might be slight changes in the details. In addition, a set of calculations was performed for the subcritical case with $Re = 125$ in this geometry with $h = 1/16$, 1/24, 1/32 and 1/48. In this case the extended wave was generated for the three finer grids, but not with $h = 1/16$, i.e. in practice the diffusive effect of the grid-related truncation error for $h = 1/16$ was sufficient to drop the effective Reynolds number below the critical Reynolds number for the generation of the extended wave *for this geometry* (note that for $Re = 120$ we did not obtain an extended wave in this channel for any value of h). The diffusive effect of the truncation error is not unexpected, but we note, however, that if a grid of $h = 1/32$ rather than $h = 1/48$ had been used throughout the calculations, the same conclusions would have been drawn concerning the existence and general form and behaviour of the wave, although there would be some change in the details (e.g. the strength of the wave and the occurrence of secondary separation on the walls). In particular, no case was found where there was an extended wave for a crude grid which disappeared as the grid was refined.

5. Discussion

Above we have presented numerical solutions of the steady Navier–Stokes equations for the flow in non-uniform channels in which JH flow might be expected, subject to stability considerations. We have concentrated on flow near $\mathscr{B}_2$, which previous studies (Sobey & Drazin 1986; Banks *et al.* 1988) have given as the boundary for the spatial stability of JH flow. In general our results support this conjecture, and show that near $\mathscr{B}_2$ small changes in geometry or the Reynolds number can cause very large changes in the flow.

For all combinations of (Re, α) above $\mathscr{B}_2$, a disturbance to the flow developed in the streamwise direction, leading ultimately to a large-amplitude wave of constant wavelength and strength when viewed in the appropriate coordinate system. Below $\mathscr{B}_2$ the situation was not as simple: for a channel with a change in the slope of the wall(s) at $x = 0$, but no step(s), JH flow was obtained just below $\mathscr{B}_2$, but not just above.

In contrast, when the channel doubles in width at $x = 0$, the extended non-linear wave was generated for both symmetric and asymmetric channels at points in the parameter space significantly below $\mathscr{B}_2$ (e.g. $\alpha = 2°$, $Re = 125$). This last result is consistent with several predictions of Sobey & Drazin (1986) and Banks *et al.* (1988), namely the importance of the upstream boundary conditions and the subcritical nature of the pitchfork bifurcation/stability limit at $\mathscr{B}_2$. Banks *et al.* also found that the boundary conditions at infinity (the outlet) affected the stability characteristics of the flow. However, in our calculations the effect of the downstream condition was strictly local, e.g. for $\epsilon = 2$, $Re = 125$, and $\alpha = 2°$, the same flow was found over most of the channel whether or not the channel reverted to a parallel geometry at the outlet. Also, Banks *et al.* argued that for a channel with slowly varying walls, if $\alpha(x)$ does not exceed $\alpha_2(Re)$ either by too much or too far downstream, a *weakly non-linear* asymmetric disturbance may grow but would ultimately decay downstream where $\alpha(x) < \alpha_2(Re)$. Our results do not contradict this, but do suggest that if the disturbance grows to its final non-linear form then it will persist rather than decay unless $\alpha(x)$ drops significantly below $\alpha_2(Re)$.

In contrast to Sobey & Drazin's (1986) finding that the critical bifurcation at $\mathscr{B}_2$ is subcritical, Hamadiche *et al.* (1994) performed a non-linear analysis of JH flow in a finite-length channel and obtained a supercritical loss of stability, with no trace of a subcritical instability. However, while Hamadiche *et al.'s* particular problem may be supercritical, this result may not extend to JH flow in general for a number of reasons. First, their basic JH flow was symmetric, whereas Sobey & Drazin stated that while the symmetric II_1 flow is stable subcritically and the symmetric II_2 flow unstable supercritically, it is the asymmetric IV_1 and V_1 flows that are unstable subcritically. A more important question, perhaps, is whether the geometry and boundary conditions used by Hamadiche *et al.* will allow a full non-linear disturbance to develop. They presented non-linear results for two cases, $\alpha = 0.1$ rad with $r_d^*/r_u^* = 10^3$, and $\alpha = 0.3$ rad with $r_d^*/r_u^* = 10^2$, where r_u^* and r_d^* give the positions of the upstream and downstream boundaries, respectively. Using the asymptotic form of the coordinate transformation in (3.5), a channel with $r_u^* \leqslant r^* \leqslant r_d^*$ in physical space maps to one of length $X_d - X_u = \ln(r_d^*/r_u^*)/2\alpha$ in computational space. Thus Hamadiche *et al.'s* channels are in turn approximately 35 and 8 long in our computational space, much shorter than the channels of length 160 to 320 used in our calculations. The results presented above suggest that their channels are simply too short to allow the full non-linear development of the disturbance, particularly near $\mathscr{B}_2$ when there is no change in the width of the channel to abruptly initiate the full non-linear response. In addition, we have performed calculations in a channel with $\alpha = 0.1$ rad (5.73°), $\epsilon = 2$ and $X_{max} = 240$, with both sub- and supercritical Reynolds numbers (45 and 50 respectively), and in both cases an extended wave was obtained (table 1). Also, Hamadiche *et al.* calculated a non-linear perturbation to symmetric JH flow where the perturbation was either zero at the inlet and outlet or 'periodic' on the computational domain. In general, Hamadiche *et al.*'s conditions do not appear to be compatible with our solutions once the wave has developed fully, except possibly in extremely long channels in which there is room for the wave to grow and decay near the inlet and outlet, respectively, or, with periodic conditions, where the length of the channel is an integer multiple of the wavelength, which is not known *a priori*.

The wavelengths obtained in our Navier–Stokes solutions were compared with those predicted by the linear theory of Banks *et al.* (1986), using their equation (3.3). No agreement was found: for example, with $\alpha = 2°$ and $Re = 150$ the non-

linear wavelength was approximately $2\frac{1}{2}$ times that predicted by the linear theory using a II_2 JH flow, while for the (subcritical) case with $\alpha = 2°$ and $Re = 125$, the unstable linear modes obtained with IV_1/V_1 have real eigenvalues, i.e. they were non-oscillatory. Further, we are doubtful whether any linear theory will predict the final non-linear wavelength correctly as much of the development of the wave appears to be a non-linear process. A number of calculations were performed using the implicit unsteady version of the Navier–Stokes code (see Tutty & Pedley 1993 for details) to produce a time-accurate solution with the flow rate ramped up from zero. In these calculations the initial disturbance has a much shorter wavelength than that shown in e.g. figure 7, and non-linear effects were clearly significant long before the wave reached a steady state. In particular, there was a large-scale displacement of the core flow and significant eddies on the walls during much of the growth in the wavelength. Also, we note that for most of the runs the iterative process in the steady calculations mimicked this unsteady behaviour, i.e. a large-scale disturbance with a relatively short wavelength formed long before the calculation was fully converged.

Because of numerical difficulties with the unsteady code (the inner iterative process failed to converge if the Jacobian of the mapping between the physical and computational spaces became too large), the channels used in the unsteady calculations were much shorter ($0 \leqslant X \leqslant 85$) than those used for the direct steady calculations. However, they were sufficiently long to confirm that both flows with and without the extended wave could be obtained through an unsteady process in which the flow is accelerated from zero to a constant mass flow rate. In particular, the upstream portion of the extended wave was found for the subcritical case with $\alpha = 2°$, $Re = 125$, and $\epsilon = 2$, as in the steady case.

In this paper, a flow has been described as unstable if the flow far down the channel is not one of the possible JH flows. This does not of course imply that the cases in which a JH flow was obtained would necessarily be stable to unsteady modes, although when a JH flow was obtained without explicitly forcing the flow to be symmetric, it was a symmetric unidirectional flow, found by Sobey & Drazin (1986) to be subcritically stable.

The flow pattern found when the extended wave occurs is markedly different from the usual steady flow in a channel with an expansion in the form of a backward-facing step, where, if a wave exists, it decays rapidly downstream (see e.g. Armaly *et al.* 1983; Sobey 1985). The individual flow structures in the extended wave have a characteristic pattern, with a large-amplitude displacement of the core flow with eddies generated successively on the lower and upper wall, and more vigorous flow and a concentration of vorticity towards the downstream ends of the eddies, leading to, at higher *Re*, secondary separation on the wall upstream of the main core of each eddy (see figure 14*c*). These flow structures strongly resemble those found in unsteady flow in non-uniform channels, when a 'vortex wave' is generated by decelerating flow over an expansion or through a constriction (see e.g. Sobey 1985; Tutty 1992; Tutty & Pedley 1993). In addition to the flow patterns, the unsteady and steady results agree in a number of aspects: in both cases the waves are generated when the flow is decelerating, and, for a given geometry, the waves are relatively weak and limited in extent for 'low' *Re* (Tutty & Pedley 1993).

This work was supported by the UK Engineering and Physical Sciences Research Committee through the computational facilities used for all the calculations performed in the study.

REFERENCES

ARMALY, B. F., DURST, F., PEREIRA, J. C. F. & SCHONUNG, B. 1983 Experimental and theoretical investigation of a backward-facing step flow. *J. Fluid Mech.* **127**, 473–496.

BANKS, W. H. H., DRAZIN, P. G. & ZATURSKA, M. B. 1988 On perturbations of Jeffery–Hamel flow. *J. Fluid Mech.* **186**, 559–581.

BUITRAGO, S. E. 1983 Detailed analysis of higher Jeffery–Hamel solutions. M.Phil. thesis, University of Sussex.

FRAENKEL, L. E. 1962 Laminar flow in symmetrical channels with slightly curved walls. I. On the Jeffery–Hamel solutions for flow between plane walls. *Proc. R. Soc. Lond.* A **267**, 119–138.

FRAENKEL, L. E. 1963 Laminar flow in symmetrical channels with slightly curved walls. II. An asymptotic series for the streamfunction. *Proc. R. Soc. Lond.* A **272**, 406–428.

HAMADICHE, M., SCOTT, J. & JEANDEL, D. 1994 Temporal stability of Jeffery–Hamel flow. *J. Fluid Mech.* **268**, 71–88.

HAMEL, G. 1916 Spiralfömrige Bewegungen zäher Flüssigkeiten. *Jahresbericht der Deutschen Math. Vereinigung* **25**, 34–60.

JEFFERY, G. B. 1915 The two-dimensional steady motion of a viscous fluid. *Phil. Mag* (6) **29**, 455–465.

PEDLEY, T. J. & STEPHANOFF, K. D. 1985 Flow along a channel with a time-dependent indentation in one wall: the generation of vorticity waves. *J. Fluid Mech.* **160**, 337–367.

SOBEY, I. J. 1985 Observations of waves during oscillatory channel flow. *J. Fluid Mech.* **151**, 395–426.

SOBEY, I. J. & DRAZIN, P. G. 1986 Bifurcation of two-dimensional channel flows. *J. Fluid Mech.* **171**, 263–287.

TUTTY, O. R. 1992 Pulsatile flow in a constricted channel. *Trans ASME: J. Biomech. Engng* **114**, 50–54.

TUTTY, O. R. & PEDLEY, T. J. 1993 Oscillatory flow in a stepped channel. *J. Fluid Mech.* **247**, 179–204.